

EEG-based Graph-guided Domain Adaptation for Robust Cross-Session Emotion Recognition

Maryam Mirzaei, Farzaneh Shayegh, Hamed Narimani

Abstract—Accurate recognition of human emotional states is critical for effective human–machine interaction. Electroencephalography (EEG) offers a reliable source for emotion recognition due to its high temporal resolution and its direct reflection of neural activity. Nevertheless, variations across recording sessions present a major challenge for model generalization. To address this issue, we propose EGDA, a framework that reduces cross-session discrepancies by jointly aligning the global (marginal) and class-specific (conditional) distributions, while preserving the intrinsic structure of EEG data through graph regularization. Experimental results on the SEED-IV dataset demonstrate that EGDA achieves robust cross-session performance, obtaining accuracies of 81.22%, 80.15%, and 83.27% across three transfer tasks, and surpassing several baseline methods. Furthermore, the analysis highlights the Gamma frequency band as the most discriminative and identifies the central-parietal and prefrontal brain regions as critical for reliable emotion recognition.

Index Terms—Domain adaptation, EEG, Emotion recognition, Frequency band analysis, Graph learning, Transfer learning.

I. INTRODUCTION

ACCURATE recognition of human emotions is essential for developing effective human–machine interaction systems [1]. Over the past decade, numerous studies have explored emotion recognition using various sources, such as vision-based, text-based, and speech-based approaches [2]. While these non-physiological methods are relatively easy to implement, they suffer from limited reliability, as individuals can deliberately disguise their facial expressions, vocal tones, or textual sentiment [3].

Among physiological signals, EEG has emerged as one of the most informative sources for emotion recognition. EEG directly reflects neural activity with high temporal resolution and reflects the dynamics of cognitive and affective processes in the brain [4]. Despite promising progress, EEG-based emotion recognition faces critical challenges. A major difficulty arises from the non-stationarity of EEG signals, as their distributions vary across recording sessions, subjects, and environmental conditions [5]. In particular, even for the same subject, data collected on different sessions may exhibit significant distributional shifts due to changes in mental state, electrode placement, or environmental noise [5], [6]. Consequently, models trained on one session often perform poorly when applied to another, limiting generalization. This challenge motivates the development of cross-session domain adaptation techniques that can transfer knowledge from a labeled source session to an unlabeled [7].

Several approaches focus on EEG-based emotion recognition using graph-based models to capture the structural relationships among samples [8]. However, these models do not employ transfer learning to address distribution mismatches across sessions or subjects. As a result, while they effectively model inter-sample similarity, they overlook aligning feature distributions between different domains.

To address these issues, we propose a framework termed EGDA. By integrating domain adaptation with graph-based regularization, EGDA simultaneously reduces both marginal (feature-level) and conditional (class-conditional) distribution discrepancies while preserving the intrinsic geometric and semantic structures of EEG data. Specifically, EGDA leverages an iterative pseudo-labeling strategy to refine class-level alignment and employs a Laplacian graph to maintain neighborhood consistency during the adaptation process. This unified framework enables robust cross-session emotion recognition performance.

The contributions of this work are summarized as follows:

- We formulate a graph-guided domain adaptation framework for cross-session EEG emotion recognition, in which structural relationships among EEG samples are explicitly incorporated into the adaptation objective to preserve neighborhood consistency across sessions.
- We introduce a source-domain within-class scatter minimization constraint to preserve class discriminability and stabilize the adaptation process under cross-session distribution shifts.
- We formulate a unified subspace learning model with graph-based regularization that jointly aligns marginal and conditional distributions; the conditional alignment is iteratively refined via pseudo-label updates regularized by neighborhood structure and within-class scatter constraints, without requiring labeled target data.

The remainder of this paper is organized as follows. Section II reviews related works in EEG-based emotion recognition and transfer learning. Section III presents the formulation and optimization of the proposed model. Section IV describes the experimental setup, results, and performance analysis. Finally, Section V concludes the paper.

Notations: Uppercase bold letters denote matrices, while lowercase bold letters denote vectors. For a matrix \mathbf{A} , \mathbf{a}^i and \mathbf{a}_j denote its i -th row and j -th column, respectively, and a_{ij} denotes the element at the i -th row and j -th column. The superscript $(\cdot)^c$ indicates quantities associated with class c .

II. RELATED WORK

This section reviews two categories of closely related studies: (1) EEG-based emotion recognition models evaluated

on the SEED-IV dataset, and (2) transfer learning and domain adaptation approaches relevant to the proposed EGDA framework. Since EGDA is a domain adaptation model, both categories are relevant for positioning our contributions.

A. SEED-IV-Based emotion recognition methods

GFIL proposes a unified importance learning framework for EEG-based emotion recognition by jointly performing emotion classification and feature importance estimation within a least-squares regression formulation [9]. By introducing an auto-weighting mechanism, GFIL enables to automatically learn the relative contributions of different EEG feature dimensions, providing both improved recognition performance and enhanced interpretability.

JSFA introduces a joint sample and feature importance assessment framework for EEG-based emotion recognition by integrating self-paced learning with feature self-weighting into a least-squares regression model [10]. The self-paced mechanism adaptively down-weights low-quality or noisy EEG samples.

Graph-based semi-supervised learning has been widely explored to exploit the intrinsic structural relationships among EEG samples. OGSSL proposes a unified framework that jointly learns an optimal graph structure and infers emotional labels for unlabeled EEG samples, enabling mutual reinforcement between graph construction and semi-supervised classification [11].

SRAGL proposes a semi-supervised regression framework with adaptive graph learning for cross-session EEG-based emotion recognition [12]. It jointly estimates the emotional labels of unlabeled samples and learns a sample similarity graph within a unified optimization process, allowing the graph structure and label inference to mutually reinforce each other. By iteratively updating the regression model and graph adjacency matrix, SRAGL aims to capture the intrinsic relationships among EEG samples and improve emotion recognition performance across sessions.

GASDL proposes a graph-adaptive semi-supervised discriminative subspace learning framework for EEG-based emotion recognition [13]. It jointly learns a discriminative subspace by minimizing intra-class scatter while preserving local sample relationships through an adaptively constructed maximum-entropy graph. The graph learning, subspace projection, and pseudo-label estimation are tightly coupled within a unified optimization process, enabling mutual reinforcement between structural modeling and label inference. However, the iterative updating of neighborhood relationships may introduce graph instability, particularly in noisy or cross-session EEG scenarios.

CPTML proposes a coupled projection transfer metric learning framework for cross-session EEG-based emotion recognition, aiming to address both cross-session and cross-trial distribution discrepancies [14]. It jointly integrates domain alignment and graph-based metric learning into a unified optimization objective, where domain alignment extracts domain-invariant features while metric learning enforces discriminative relationships among EEG samples belonging to the same

emotional state. By coupling these two components, CPTML enables mutual reinforcement between data alignment and similarity modeling, leading to improved recognition performance across sessions. Nevertheless, the coupled optimization procedure can be computationally demanding, which may affect scalability in practical EEG applications.

JAGP addresses cross-subject EEG emotion recognition by unifying domain-invariant feature adaptation, graph-adaptive label propagation, and emotion estimation within a single objective function [15]. The graph structure is iteratively updated based on the shared subspace representations, allowing label propagation and feature alignment to mutually reinforce each other. However, as both graph construction and feature adaptation depend on intermediate pseudo-labels, errors in label estimation may propagate through iterations and affect the robustness of the learned representations.

B. Transfer Learning Approaches

TCA is a feature-based unsupervised domain adaptation method that learns a shared subspace by minimizing the discrepancy between source and target marginal distributions using MMD [16]. By projecting data into transfer components, TCA reduces domain shift at the distribution level. However, TCA does not explicitly account for class-conditional distribution differences and does not exploit source label information, which may limit its effectiveness when conditional distributions vary significantly across domains.

JDA extends TCA by explicitly aligning both marginal and conditional distributions between source and target domains within a unified subspace learning framework [17]. It leverages pseudo-labels for the target domain to estimate class-conditional discrepancies and iteratively refines the shared representation. While JDA achieves improved adaptation performance, its reliance on pseudo-label quality may affect robustness under severe distribution shifts.

VDA further addresses large domain shifts by jointly reducing marginal and conditional distribution discrepancies while promoting class discrimination through domain-invariant clustering [18]. By integrating distribution adaptation with within-class scatter minimization, VDA learns a discriminative and transferable representation.

Collectively, these methods demonstrate that distribution alignment effectively reduces inter-session variability. Building on this foundation, our work integrates robust graph learning with transfer alignment to better preserve discriminative features.

III. PROPOSED METHOD

A. Preliminary

Let $\mathcal{D}_s = \{\mathbf{X}_s, \mathbf{Y}_s\}$ denote the labeled source domain with n_s samples, and $\mathcal{D}_t = \{\mathbf{X}_t\}$ denote the unlabeled target domain with n_t samples. Here, $\mathbf{X}_s \in \mathbb{R}^{d \times n_s}$ and $\mathbf{X}_t \in \mathbb{R}^{d \times n_t}$ represent the EEG feature matrices of the source and target domains, respectively, where d is the feature dimensionality. The label matrix of the source domain is denoted by $\mathbf{Y}_s \in \mathbb{R}^{C \times n_s}$, with C being the number of emotion

classes and each column of \mathbf{Y}_s is a one-hot encoded label vector corresponding to a source sample.

We further define the combined feature matrix as $\mathbf{X} = [\mathbf{X}_s, \mathbf{X}_t] \in \mathbb{R}^{d \times n}$, where $n = n_s + n_t$ is the total number of samples.

We assume that the source and target domains share the same feature space and label space, i.e., $\mathcal{X}_s = \mathcal{X}_t$ and $\mathcal{Y}_s = \mathcal{Y}_t$. Here, \mathcal{X} denotes the d -dimensional EEG feature space, and \mathcal{Y} denotes the label space. However, due to domain shift, the source and target domains follow different data distributions. Specifically, their marginal distributions over the feature space and conditional distributions over the labels may differ, i.e., $P_s(x) \neq P_t(x)$ and $P_s(y|x) \neq P_t(y|x)$.

To mitigate distribution discrepancy between domains, a linear projection matrix $\mathbf{A} \in \mathbb{R}^{d \times d_f}$ is learned, where d and $d_f \leq d$ denote the original and projected feature dimensionalities, respectively. The projection \mathbf{A}^T maps the source and target features to a shared subspace, yielding $\mathbf{A}^T \mathbf{X}_s$ and $\mathbf{A}^T \mathbf{X}_t$. This shared representation facilitates better alignment of marginal and conditional distributions while preserving discriminative information for emotion recognition.

B. Problem Statement

Given a labeled source-domain EEG dataset $\mathcal{D}_s = \{\mathbf{X}_s, \mathbf{Y}_s\}$ and an unlabeled target-domain EEG dataset $\mathcal{D}_t = \{\mathbf{X}_t\}$ collected from different sessions, the goal of this work is to learn a transferable model that can accurately recognize emotional states in the target domain. Due to distribution discrepancies across sessions, models trained on the source domain often generalize poorly to the target domain. Moreover, the absence of target labels makes direct supervised learning infeasible. Therefore, the key challenge is to jointly reduce cross-session distribution mismatch while inferring reliable target-domain labels, without access to labeled target data.

C. Model Formulation

In this paper, we propose a joint adaptation framework that learns a low-dimensional representation $\mathbf{A} \in \mathbb{R}^{d \times d_f}$ and simultaneously improving the target-domain labels. Since the target domain is unlabeled (i.e., $P_t(\mathbf{Y}_t|\mathbf{X}_t)$ cannot be directly observed), we employ an EM-like strategy that iteratively updates both the the projection matrix and the target pseudo-labels..

A central goal of transfer learning is to reduce distributional divergence between source and target domains. In EEG-based emotion recognition, session variability, noise, and experimental conditions cause distribution shifts, which degrade the performance of classifiers trained solely on source data. To address this, EGDA learns a linear projection matrix \mathbf{A} that maps both domains into a shared subspace where their marginal distributions are close. This principle can be implemented by the following objective function:

$$\min_{\mathbf{A}} \left\| \frac{1}{n_s} \sum_{i=1}^{n_s} \mathbf{A}^T \mathbf{x}_{si} - \frac{1}{n_t} \sum_{j=1}^{n_t} \mathbf{A}^T \mathbf{x}_{tj} \right\|^2. \quad (1)$$

This can be expressed in matrix form as:

$$\min_{\mathbf{A}} \text{Tr}(\mathbf{A}^T \mathbf{X} \mathbf{M}_0 \mathbf{X}^T \mathbf{A}), \quad (2)$$

where \mathbf{M}_0 is MMD coefficient matrix:

$$(\mathbf{M}_0)_{ij} = \begin{cases} \frac{1}{n_s^2}, & \mathbf{x}_i, \mathbf{x}_j \in \mathbf{X}_s, \\ \frac{1}{n_t^2}, & \mathbf{x}_i, \mathbf{x}_j \in \mathbf{X}_t, \\ \frac{-1}{n_s n_t}, & \text{otherwise.} \end{cases} \quad (3)$$

Geometrically, this ensures that the Euclidean distance between the source and target domain centers in the latent space is minimized.

Aligning only marginal distributions does not guarantee semantic consistency across domains, since it ignores class information and can lead to samples from different classes being mapped close to each other in the latent space. Consequently, class-conditional misalignment may still exist, especially in noisy EEG data. To address this issue, EGDA aligns conditional distributions for each class using pseudo-labels for target samples.

The class-wise alignment is defined as:

$$\min_{\mathbf{A}} \sum_{c=1}^C \left\| \frac{1}{n_s^{(c)}} \sum_{\mathbf{x}_i \in \mathbf{X}_s^{(c)}} \mathbf{A}^T \mathbf{x}_i - \frac{1}{n_t^{(c)}} \sum_{\mathbf{x}_j \in \mathbf{X}_t^{(c)}} \mathbf{A}^T \mathbf{x}_j \right\|^2 \quad (4)$$

$n_s^{(c)}$ and $n_t^{(c)}$ denote the number of samples in the source and target domains that belong to the class c , respectively. Also, $\mathbf{X}_s^{(c)}$ and $\mathbf{X}_t^{(c)}$ are defined to be the set of instances from class c belonging to the source and target data in turn.

This can be expressed in matrix form as:

$$\min_{\mathbf{A}} \text{Tr}(\mathbf{A}^T \mathbf{X} \mathbf{M}_c \mathbf{X}^T \mathbf{A}), \quad (5)$$

where, $\mathbf{M}_c \in \mathbb{R}^{n \times n}$ is MMD coefficient matrix:

$$(\mathbf{M}_c)_{ij} = \begin{cases} \frac{1}{(n_l^{(c)})^2} & \mathbf{x}_i, \mathbf{x}_j \in \mathbf{X}_l^{(c)} \\ \frac{1}{(n_t^{(c)})^2} & \mathbf{x}_i, \mathbf{x}_j \in \mathbf{X}_t^{(c)} \\ -\frac{1}{n_l^{(c)} n_t^{(c)}} & \mathbf{x}_i \in \mathbf{X}_l^{(c)}, \mathbf{x}_j \in \mathbf{X}_t^{(c)} \\ -\frac{1}{n_t^{(c)} n_l^{(c)}} & \mathbf{x}_j \in \mathbf{X}_l^{(c)}, \mathbf{x}_i \in \mathbf{X}_t^{(c)} \\ 0 & \text{otherwise} \end{cases} \quad (6)$$

To enhance separability in the latent space, samples belonging to the same class in the source domain should form compact clusters. This property can be enforced by minimizing the within-class scatter matrix, defined as:

$$\mathbf{S}_w = \sum_{c=1}^C \sum_{\mathbf{x}_i \in \mathbf{X}_s^{(c)}} (\mathbf{x}_i - \boldsymbol{\mu}_c)(\mathbf{x}_i - \boldsymbol{\mu}_c)^T, \quad (7)$$

where $\boldsymbol{\mu}_c$ is the mean vector of class c in the source domain, computed as:

$$\boldsymbol{\mu}_c = \frac{1}{n_s^{(c)}} \sum_{\mathbf{x}_i \in \mathbf{X}_s^{(c)}} \mathbf{x}_i, \quad (8)$$

and $n_s^{(c)}$ denotes the number of source samples in class c .

To encourage the compactness of intra-class representations, EGDA formulates the following objective:

$$\min_{\mathbf{A}} \text{Tr}(\mathbf{A}^T \mathbf{S}_w \mathbf{A}). \quad (9)$$

To model local relationships among samples, we construct an adaptive similarity graph represented by a weight matrix $\mathbf{S} \in \mathbb{R}^{n \times n}$, where each element s_{ij} quantifies the similarity between samples \mathbf{x}_i and \mathbf{x}_j . Intuitively, samples that are closer in Euclidean distance are more likely to belong to the same class and are therefore assigned higher similarity weights, whereas more distant samples receive smaller weights to reflect weaker relationships.

The similarity learning problem is formulated as:

$$\min_{s_{ij} \geq 0, \mathbf{s}^i \mathbf{1} = 1} \sum_{i,j=1}^n \|\mathbf{x}_i - \mathbf{x}_j\|_2^2 s_{ij}, \quad (10)$$

where \mathbf{s}^i denotes the i -th row of the similarity matrix \mathbf{S} , and $\mathbf{1} \in \mathbb{R}^n$ is the all-ones vector.

However, problem (10) may lead to a trivial solution in which only one element of \mathbf{s}^i equals one while all others are zero [19]. Although this minimizes the objective, it produces a degenerate graph where each sample is connected only to its nearest neighbor. This fails to capture the local manifold structure and undermines graph-based regularization. To address this, a regularization term is introduced:

$$\begin{aligned} \min_{\mathbf{S}} \sum_{i,j=1}^n & \left(\|\mathbf{x}_i - \mathbf{x}_j\|_2^2 s_{ij} + \gamma s_{ij}^2 \right) \\ \text{s.t. } & s_{ij} \geq 0, \mathbf{s}^i \mathbf{1} = 1. \end{aligned} \quad (11)$$

Here, γ is a control parameter that regulates the dispersion of values. A smaller γ yields highly localized similarity weights, whereas a larger γ produces more evenly distributed weights, improving stability in the presence of noise.

Since each row \mathbf{s}^i depends only on distances involving sample i , problem (11) can be decomposed into n independent row-wise subproblems:

$$\begin{aligned} \min_{\mathbf{S}} \sum_{j=1}^n & \left(\|\mathbf{x}_i - \mathbf{x}_j\|_2^2 s_{ij} + \gamma s_{ij}^2 \right) \\ \text{s.t. } & s_{ij} \geq 0, \mathbf{s}^i \mathbf{1} = 1. \end{aligned} \quad (12)$$

Define $m_{ij} = \|\mathbf{x}_i - \mathbf{x}_j\|_2^2$, and let $\mathbf{m}^i \in \mathbb{R}^{1 \times n}$ denote the vector whose j -th element is m_{ij} . Under this notation, problem (11) can be rewritten in the following row-wise form:

$$\begin{aligned} \min_{\mathbf{S}} & \left\| \mathbf{s}^i + \frac{\mathbf{m}^i}{2\gamma} \right\|_2^2 \\ \text{s.t. } & s_{ij} \geq 0, \mathbf{s}^i \mathbf{1} = 1. \end{aligned} \quad (13)$$

This reformulation indicates that \mathbf{s}^i is obtained by projecting $-\frac{\mathbf{m}^i}{2\gamma}$ onto the probability simplex, which enforces non-negativity and unit-sum constraints on each row. As discussed in [19], this projection yields the closest feasible similarity vector under these constraints.

Since EEG data are often noisy and redundant, it is advantageous to learn the similarity matrix in a lower-dimensional

subspace. Let $\mathbf{A} \in \mathbb{R}^{d \times d_f}$ be a linear projection matrix. The similarity learning problem is then extended as:

$$\begin{aligned} \min_{\mathbf{S}, \mathbf{A}} & \sum_{i,j=1}^n \left(\|\mathbf{A}^T \mathbf{x}_i - \mathbf{A}^T \mathbf{x}_j\|_2^2 s_{ij} + \gamma s_{ij}^2 \right) \\ \text{s.t. } & s_{ij} \geq 0, \mathbf{s}^i \mathbf{1} = 1. \end{aligned} \quad (14)$$

Once \mathbf{S} is estimated, the resulting graph is used to compute the Laplacian matrix:

$$\mathbf{L}_s = \mathbf{D}_s - \frac{\mathbf{S} + \mathbf{S}^T}{2}, \quad (15)$$

where \mathbf{D}_s is diagonal with entries $d_{ii} = \sum_j s_{ij}$.

The first term of (14) can be written in matrix form as [9]:

$$\sum_{i,j=1}^n \|\mathbf{A}^T \mathbf{x}_i - \mathbf{A}^T \mathbf{x}_j\|_2^2 s_{ij} = \text{Tr}(\mathbf{A}^T \mathbf{X} \mathbf{L}_s \mathbf{X}^T \mathbf{A}), \quad (16)$$

while the second term can be expressed as:

$$\sum_{i,j=1}^n s_{ij}^2 = \|\mathbf{S}\|_F^2 = \text{Tr}(\mathbf{S}^T \mathbf{S}), \quad (17)$$

Therefore, the matrix form of problem (14) is given by:

$$\min_{\mathbf{A}, \mathbf{S}} \text{Tr}(\mathbf{A}^T \mathbf{X} \mathbf{L}_s \mathbf{X}^T \mathbf{A} + \gamma \mathbf{S}^T \mathbf{S}). \quad (18)$$

To prevent overfitting and ensure generalizable solutions, Frobenius norm regularization is applied:

$$\min_{\mathbf{A}} \|\mathbf{A}\|_F^2 = \min_{\mathbf{A}} \text{Tr}(\mathbf{A}^T \mathbf{A}). \quad (19)$$

This penalizes large values in the projection matrix, encouraging smoother, more robust representations and avoiding fitting noise in the EEG data.

By integrating all components, the final optimization problem is formulated as:

$$\begin{aligned} \min_{\mathbf{A}, \mathbf{S}} & \alpha \sum_{c=0}^C \text{Tr}(\mathbf{A}^T \mathbf{X} \mathbf{M}_c \mathbf{X}^T \mathbf{A}) + \beta \text{Tr}(\mathbf{A}^T \mathbf{S}_w \mathbf{A}) \\ & + \mu \text{Tr}(\mathbf{A}^T \mathbf{X} \mathbf{L}_s \mathbf{X}^T \mathbf{A}) + \lambda \text{Tr}(\mathbf{A}^T \mathbf{A}) + \gamma \text{Tr}(\mathbf{S}^T \mathbf{S}) \\ \text{s.t. } & \mathbf{A}^T \mathbf{X} \mathbf{H} \mathbf{X}^T \mathbf{A} = \mathbf{I}, \quad \mathbf{S} \geq 0, \quad \mathbf{S} \mathbf{1} = 1. \end{aligned} \quad (20)$$

where $\mathbf{H} = \mathbf{I} - \frac{1}{n} \mathbf{1} \mathbf{1}^T$ is the centering matrix, and $\alpha, \beta, \mu, \lambda$, and γ are trade-off parameters controlling distribution alignment, within-class compactness, graph regularization, projection regularization, and similarity smoothness, respectively.

In the experiments, the values of the coefficients $\alpha, \beta, \gamma, \mu$, and λ were selected randomly from the set $\{0.001, 0.01, 0.1, 0.2, 0.5, 1, 2, 5, 10, 50, 100\}$ to adjust the relative importance of the corresponding terms in the objective function.

D. Model Optimization

The objective function of EGDA depends on two variables, the projection matrix \mathbf{A} and the similarity matrix \mathbf{S} . We optimize this objective using the alternating direction method, updating one variable while keeping the other fixed. The detailed update rules are as follows:

(1) \mathbf{S} Optimziation:

To update \mathbf{S} in problem (20), we optimize the projected similarity learning problem (14) while keeping \mathbf{A} fixed. Since each row \mathbf{s}^i depends only on distances involving sample i , problem (14) can be decomposed into n independent row-wise subproblems as:

$$\begin{aligned} \min_{\mathbf{S}, \mathbf{A}} & \sum_{j=1}^n \left(\|\mathbf{A}^T \mathbf{x}_i - \mathbf{A}^T \mathbf{x}_j\|_2^2 s_{ij} + \gamma s_{ij}^2 \right), \\ \text{s.t. } & s_{ij} \geq 0, \mathbf{s}^i \mathbf{1} = 1. \end{aligned} \quad (21)$$

We denote $d_{ij} = \|\mathbf{A}^T \mathbf{x}_i - \mathbf{A}^T \mathbf{x}_j\|_2^2$, and define $\mathbf{d}^i \in \mathbb{R}^{1 \times n}$ as the vector whose j -th element is d_{ij} . problem (21) can be rewritten in the following row-wise form:

$$\begin{aligned} \min_{\mathbf{S}} & \frac{1}{2} \|\mathbf{s}^i + \frac{\mathbf{d}^i}{2\gamma}\|_2^2, \\ \text{s.t. } & s_{ij} \geq 0, \mathbf{s}^i \mathbf{1} = 1. \end{aligned} \quad (22)$$

Where, \mathbf{s}^i denotes the i -th row of the similarity matrix \mathbf{S} , which is updated by solving (22). This update corresponds to a Euclidean projection onto the probability simplex and can be efficiently solved using the Lagrangian multiplier method combined with Newton's method [20].

(2) \mathbf{A} Optimziation: We can rewrite optimization problem (20) as:

$$\begin{aligned} \min_{\mathbf{A}} & \sum_{c=0}^C \text{Tr}(\mathbf{A}^T (\alpha \mathbf{X} \mathbf{M}_c \mathbf{X}^T + \beta \mathbf{S}_w + \mu \mathbf{X} \mathbf{L}_s \mathbf{X}^T + \lambda \mathbf{I}) \mathbf{A}) \\ \text{s.t. } & \mathbf{A}^T \mathbf{X} \mathbf{H} \mathbf{X}^T \mathbf{A} = \mathbf{I}, \end{aligned} \quad (23)$$

To update \mathbf{A} , we employ the method of Lagrange multipliers. Accordingly, the corresponding Lagrangian function is defined as follows:

$$\begin{aligned} \mathcal{L}(\mathbf{A}) = & \text{Tr} \left(\mathbf{A}^T (\alpha \mathbf{X} \mathbf{M}_c \mathbf{X}^T + \mu \mathbf{X} \mathbf{L}_s \mathbf{X}^T + \beta \mathbf{S}_w + \lambda \mathbf{I}) \mathbf{A} \right) \\ & + \text{Tr} \left(\Phi (\mathbf{I} - \mathbf{A}^T \mathbf{X} \mathbf{H} \mathbf{X}^T \mathbf{A}) \right). \end{aligned} \quad (24)$$

where $\Phi \in \mathbb{R}^{d \times d}$ is a diagonal matrix of Lagrange multipliers [21].

Taking the derivative of the Lagrangian with respect to \mathbf{A} and setting it to zero, the following equation is obtained:

$$\begin{aligned} & (\alpha \mathbf{X} \mathbf{M}_c \mathbf{X}^T + \beta \mathbf{S}_w + \mu \mathbf{X} \mathbf{L}_s \mathbf{X}^T + \lambda \mathbf{I}) \mathbf{A} \\ & = \mathbf{X} \mathbf{H} \mathbf{X}^T \mathbf{A} \Phi. \end{aligned} \quad (25)$$

Let

$$\mathbf{P} = \alpha \mathbf{X} \mathbf{M}_c \mathbf{X}^T + \beta \mathbf{S}_w + \mu \mathbf{X} \mathbf{L}_s \mathbf{X}^T + \lambda \mathbf{I}, \quad \mathbf{Q} = \mathbf{X} \mathbf{H} \mathbf{X}^T,$$

For notational convenience, the generalized eigenvalue problem can be written as:

$$\mathbf{P} \mathbf{A} = \mathbf{Q} \mathbf{A} \Phi. \quad (26)$$

The columns of \mathbf{A} are the generalized eigenvectors, and the diagonal entries of Φ are the corresponding eigenvalues. To minimize the objective, we select the d_f eigenvectors associated with the smallest eigenvalues. Equivalently, \mathbf{A} can be obtained from the d_f eigenvectors of $\mathbf{Q}^{-1} \mathbf{P}$ corresponding to the smallest eigenvalues, assuming the null space of \mathbf{X} has been removed so that \mathbf{Q} is invertible.

After projecting the data into the learned subspace \mathbf{A} , a classifier (e.g., nearest neighbor) assign pseudo-labels to the target samples. These pseudo-labels are then used to update \mathbf{M}_c and \mathbf{S} , refining class-wise distribution alignment. This procedure is repeated for a fixed number of iterations (typically 10–20). At each iteration, EGDA integrates pseudo-label updating with an EM-like optimization strategy, progressively improving the target label estimates.

Based on the above analysis, the whole procedure of EGDA is summarized in Algorithm 1.

Algorithm 1 EEG-based Graph Domain Adaptation for Robust Cross-Session EEG Emotion Recognition (EGDA).

Input: $\{\mathbf{X}_l, \mathbf{Y}_l\}$, target \mathbf{X}_t ; parameters $\alpha, \beta, \mu, \lambda, \gamma$; subspace dimension d_f .
Output: Predicted labels of the target samples \mathbf{Y}_u and projection matrix \mathbf{A} ;
 Initialize \mathbf{S} by solving (11);
 Calculate the Laplacian matrix according to (15);
 Calculate the scatter matrix according to (7);
 Calculate the \mathbf{M}_0 according to (3) and the \mathbf{M}_c according to (6).
repeat
 Update \mathbf{A} by solving the eigendecomposition in (25) and selecting the d_f eigenvectors corresponding to the smallest eigenvalues.
 Train a classifier f on $(\mathbf{A}^T \mathbf{X}_l, \mathbf{Y}_l)$;
 Update pseudo-labels $\hat{\mathbf{Y}}_t = f(\mathbf{A}^T \mathbf{X}_t)$;
 Update \mathbf{M}_c using current pseudo-labels according to (6);
 Update \mathbf{S} according to (14);
 Recompute the Laplacian matrix according to (15).
until convergence

IV. EXPERIMENTS

In this section, we evaluate the performance of the proposed EGDA model. We first describe the EEG dataset and the preprocessing steps. Then, we present the experimental setup and conduct two types of comparisons: (1) comparisons with existing methods evaluated on the same dataset, and (2) comparisons with representative methods that share similar modeling strategies. Finally, we introduce the performance measures used for evaluation. All experiments are conducted under a subject-dependent setting, where EEG data from the same subject are used for both training and testing across different sessions.

A. Dataset Description

In this study, we conduct experiments on the publicly available SEED-IV dataset [6], which is widely used for EEG-based emotion recognition. The dataset consists of EEG recordings from 15 healthy subjects, each participating in three recording sessions conducted on different days, resulting in a total of 45 sessions. In each session, subjects viewed 24 carefully selected video clips designed to elicit four emotional states: sadness, fear, happiness, and neutrality, with six clips corresponding to each emotion.

EEG signals were acquired using 62 electrodes arranged according to the international 10–20 system. The raw signals were preprocessed and segmented into 4-second EEG samples, which serve as the basic units for feature extraction. DE features were then extracted under the assumption that EEG signals within each frequency band approximately follow a Gaussian distribution. DE features were computed from five standard frequency bands, namely Delta, Theta, Alpha, Beta, and Gamma. By concatenating DE features across all channels and frequency bands, each EEG sample is represented by a 310-dimensional feature vector. Owing to differences in video clip durations, each session contains approximately 830 EEG samples. .

B. Overall Cross-Session Performance

The proposed EGDA framework was evaluated on the SEED-IV dataset under a cross-session domain adaptation setting. EEG data from two different sessions of the same subject were used to construct each transfer task, where one session served as the labeled source domain and the other as the unlabeled target domain. Three cross-session transfer tasks were considered: Session 1→2, Session 1→3, and Session 2→3.

As shown in Tables I–III, EGDA consistently outperforms most existing methods whose performance has been previously reported on the SEED-IV dataset including GASDSL, OGSSL, SRAGL, GFIL, JSFA, CPTML and JAGP, achieving average accuracies of 81.22%, 80.15%, and 83.27% for the three transfer tasks, respectively. Although CPTML attains slightly higher accuracy in certain cases, it incurs substantially higher computational cost, which limits its applicability to large-scale or real-time scenarios. Overall, EGDA is ranked as the second-best method in terms of accuracy.

When compared with representative transfer learning methods (JDA, SDA, and VDA; Tables IV–VI), EGDA demonstrates improved recognition performance across all evaluated tasks. The results indicate that EGDA provides consistent performance gains over JDA and SDA, while exhibiting competitive performance relative to VDA. These observations suggest that EGDA is effective in preserving neighborhood structure during the domain adaptation process.

C. Emotion-Specific Recognition

To further investigate per-class recognition, Fig. 2 provides a graphical mean confusion representation of 3 trials which reveals that the neutral state is recognized with the highest accuracy (87.83%), followed by happiness (76.52%). While,

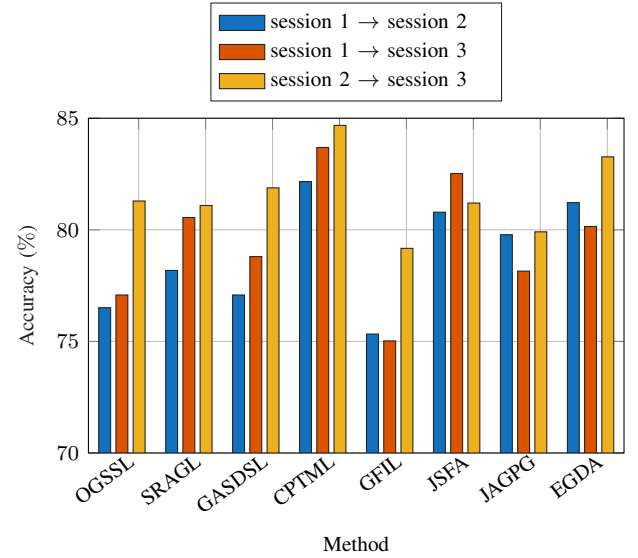


Fig. 1. Accuracies of different models for cross-session EEG emotion recognition

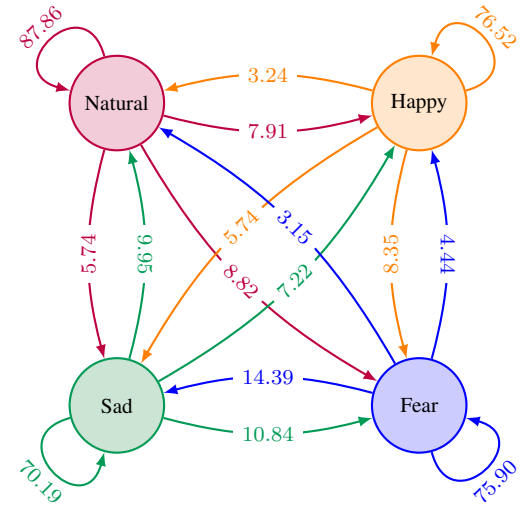


Fig. 2. The average confusion graph of EGDA for cross-session EEG emotion recognition.

fear and sadness are more prone to misclassification, with frequent confusion observed between these two negative emotional states.

D. Critical Frequency Bands and Channels Identification

In this study, EEG feature vectors are constructed by concatenating DE features extracted from multiple frequency bands and channels.

To evaluate the discriminative contribution of individual EEG features, we adopt the normalized ℓ_2 -norm of each row of the learned projection matrix \mathbf{A} as a feature importance measure. Specifically, the importance of the i -th EEG feature is defined as:

$$\theta_i = \frac{\|\mathbf{a}^i\|_2}{\sum_{j=1}^d \|\mathbf{a}^j\|_2}, \quad i = 1, 2, \dots, d, \quad \theta \in \mathbb{R}^d, \quad (27)$$

TABLE I
CROSS-SESSION (SESSION 1 → SESSION 2) EMOTION RECOGNITION RESULTS (%) OF THE EIGHT MODELS ON SEED_IV DATASET.

subject	GASDSL	OGSSL	SRAGL	CPTML	GFIL	JSFA	JAGPA	EGDA
1	80.17	65.26	65.26	88.70	66.59	75.00	88.70	80.17
2	89.06	97.36	88.94	97.36	85.70	97.36	97.36	98.80
3	77.40	75.48	79.81	91.23	67.79	84.98	91.23	88.10
4	76.32	65.99	71.27	85.94	84.98	82.93	85.94	88.58
5	69.35	69.95	68.99	88.58	75.12	80.65	88.58	81.61
6	77.16	71.39	81.37	66.95	73.32	74.76	66.95	70.43
7	79.33	85.94	82.93	94.35	94.35	95.55	94.35	89.66
8	80.89	83.05	81.13	83.97	78.97	81.85	83.97	84.13
9	80.77	78.73	82.21	73.80	79.33	82.69	73.80	75.24
10	72.48	74.88	73.44	75.24	59.25	70.19	75.24	72.12
11	68.75	67.79	69.59	64.54	69.59	66.83	64.54	59.25
12	60.58	53.25	74.16	66.11	70.07	74.76	66.11	72.00
13	66.11	75.60	72.60	72.84	70.67	69.83	72.84	68.63
14	79.63	85.70	83.65	84.01	82.21	78.73	84.01	89.66
15	94.47	97.36	97.36	98.80	93.15	95.67	98.80	100
Average	77.08	76.51	78.18	82.16	75.33	80.79	79.78	81.22

TABLE II
CROSS-SESSION (SESSION 1 → SESSION 3) EMOTION RECOGNITION RESULTS (%) OF THE EIGHT MODELS ON SEED_IV DATASET.

subject	GASDSL	OGSSL	SRAGL	CPTML	GFIL	JSFA	JAGPA	EGDA
1	75.84	80.54	73.48	84.67	74.09	69.83	79.44	84.67
2	87.23	91.85	93.43	88.69	80.54	64.84	68.61	57.18
3	83.45	66.42	67.03	74.21	75.06	78.47	71.05	65.09
4	79.83	79.68	80.05	93.07	86.74	88.69	80.78	83.21
5	73.84	52.43	65.21	85.40	66.18	85.40	76.52	80.66
6	76.64	85.89	81.39	84.79	82.12	94.28	88.81	91.36
7	88.81	91.85	96.35	80.54	79.20	96.84	86.74	89.17
8	79.56	80.90	85.04	94.89	81.02	77.13	92.82	92.94
9	75.43	77.98	79.56	80.54	70.19	75.55	75.91	80.54
10	73.48	73.97	75.30	73.51	68.61	77.37	69.34	76.28
11	78.59	78.83	80.66	85.89	71.53	83.94	72.51	78.83
12	65.94	55.84	74.94	73.51	56.57	75.67	58.34	66.30
13	74.09	64.48	73.11	63.02	57.91	63.75	64.72	62.41
14	83.73	84.31	89.66	89.54	85.28	91.73	89.42	97.69
15	85.52	91.24	93.07	92.85	90.27	92.58	97.32	95.86
Average	78.80	77.08	80.55	83.69	75.02	81.20	78.15	80.15

TABLE III
CROSS-SESSION (SESSION 2 → SESSION 3) EMOTION RECOGNITION RESULTS (%) OF THE EIGHT MODELS ON SEED_IV DATASET.

subject	GASDSL	OGSSL	SRAGL	CPTML	GFIL	JSFA	JAGP	EGDA
1	78.30	73.36	72.63	76.16	74.09	69.83	72.75	81.63
3	82.73	79.20	76.64	86.98	70.92	78.47	65.82	77.49
4	84.43	82.73	83.45	97.93	90.15	88.68	80.66	92.94
5	77.01	77.98	83.21	83.82	72.26	85.40	89.90	68.61
6	85.04	89.90	92.70	89.42	92.34	94.28	78.83	89.42
7	92.94	90.15	90.02	94.89	89.78	96.84	90.15	91.85
8	81.75	84.18	84.06	88.93	74.70	77.13	80.78	85.89
9	75.43	78.59	77.25	72.51	75.67	75.55	78.35	73.24
10	85.52	85.16	78.59	89.42	81.14	77.37	79.32	90.51
11	78.59	61.19	70.68	66.91	64.72	83.94	65.94	71.17
12	68.98	66.79	77.86	82.41	79.18	75.67	69.22	80.41
13	76.16	76.40	72.63	75.91	61.63	63.75	73.97	80.41
14	90.75	92.70	91.00	95.26	89.17	91.73	92.82	100.00
15	87.23	90.39	90.27	95.38	93.07	94.53	93.92	97.52
Average	81.88	81.29	81.99	84.68	79.17	81.20	79.78	83.27

TABLE IV
CROSS-SESSION (SESSION 1 → SESSION 2) EMOTION RECOGNITION
RESULTS (%) OF THE FOUR MODELS ON SEED_IV DATASET.

Subject	JDA	SDA	VDA	EGDA
1	63.22	70.79	80.17	80.17
2	92.55	91.23	97.36	98.80
3	68.99	69.59	84.50	88.10
4	64.30	81.37	86.06	88.58
5	71.15	59.98	70.07	81.61
6	64.98	63.22	57.81	70.43
7	73.08	85.10	92.43	89.66
8	74.04	76.20	83.41	84.13
9	72.64	59.01	70.19	75.24
10	64.18	53.25	69.11	72.12
11	62.98	63.58	53.12	59.25
12	55.41	60.94	71.15	72.00
13	64.42	61.21	66.95	68.63
14	67.79	77.76	84.86	89.66
15	93.03	95.67	100	100
Average	70.18	71.26	76.21	81.22

TABLE V
CROSS-SESSION (SESSION 1 → SESSION 3) EMOTION RECOGNITION
RESULTS (%) OF THE FOUR MODELS ON SEED_IV DATASET.

Subject	JDA	SDA	VDA	EGDA
1	62.53	77.01	83.70	84.67
2	65.33	58.52	55.47	57.18
3	53.28	42.09	68.13	65.09
4	77.74	86.25	83.33	83.21
5	70.19	72.51	78.47	80.66
6	80.90	75.79	82.85	91.36
7	56.57	85.16	87.47	89.17
8	81.75	89.42	86.50	92.94
9	58.27	52.43	81.02	80.54
10	64.84	70.21	73.24	76.28
11	66.06	67.82	68.25	78.83
12	54.26	51.70	58.15	66.30
13	56.84	40.88	65.08	62.41
14	83.82	81.39	93.92	97.69
15	80.54	78.22	92.21	95.86
Average	67.53	68.63	75.17	80.15

TABLE VI
CROSS-SESSION (SESSION 2 → SESSION 3) EMOTION RECOGNITION
RESULTS (%) OF THE FOUR MODELS ON SEED_IV DATASET.

Subject	JDA	SDA	VDA	EGDA
1	58.88	66.30	65.45	81.63
2	59.61	64.72	61.19	68.13
3	84.55	66.67	72.38	77.49
4	67.40	85.04	90.15	92.94
5	72.63	71.29	72.38	68.61
6	55.96	86.42	87.35	89.42
7	90.15	91.73	90.02	91.85
8	65.69	83.82	79.20	85.89
9	66.79	51.46	64.36	73.24
10	85.40	82.48	86.01	90.51
11	59.37	62.04	71.17	71.17
12	51.82	78.47	80.41	80.41
13	66.91	67.72	80.41	80.41
14	79.68	87.71	100	100
15	90.39	90.39	92.70	97.32
Average	70.35	75.75	77.64	83.27

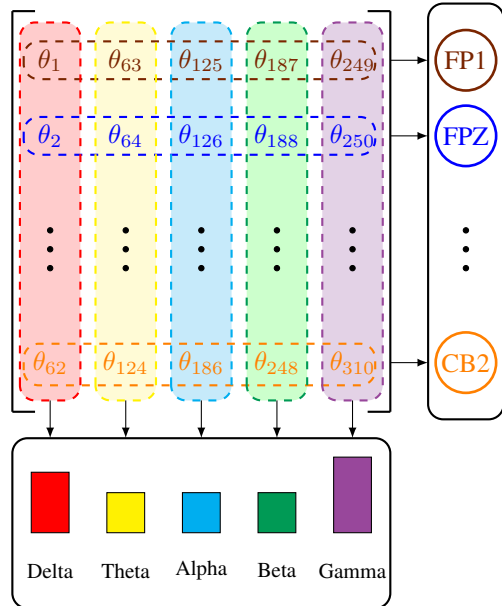


Fig. 3. Visualization of EEG feature importance with respect to frequency bands and channels.

where larger values of θ_i indicate stronger discriminative capability for distinguishing emotional states.

Based on the established correspondence between EEG feature dimensions and frequency bands/channels, the overall importance of the j -th frequency band is computed as:

$$\omega_j^{\text{band}} = \sum_{i=1}^q \theta_{(j-1) \times q + i}, \quad j = 1, 2, \dots, p, \quad (28)$$

where $p = 5$ denotes the number of frequency bands and $q = 62$ represents the number of EEG channels. Similarly, the importance of the k -th EEG channel is measured by:

$$\omega_k^{\text{channel}} = \sum_{i=1}^p \theta_{(i-1) \times q + k}, \quad k = 1, 2, \dots, q. \quad (29)$$

Since the feature representation is constructed by concatenating 62 EEG channels across 5 frequency bands, the importance vector $\theta \in \mathbb{R}^{310}$ can be reshaped into a matrix $\Theta \in \mathbb{R}^{62 \times 5}$, where each column corresponds to a frequency band and each row corresponds to an EEG channel (Fig. 3). The overall importance of each frequency band is obtained by summing the elements within the corresponding column, while the importance of each EEG channel is computed by summing the elements within the corresponding row.

The results shown in Fig. 4 illustrate the average importance of each frequency band across three cross-session trials. Among all frequency bands, the Gamma band exhibits the highest contribution to emotion recognition, followed by the Alpha band.

At the channel level, Fig. 5 presents the ten most important EEG channels averaged across the three cross-session trials. These channels are primarily located in the prefrontal, central-parietal, and bilateral temporal regions, and demonstrate the highest discriminative values (Fig. 6). Furthermore, Fig. 7 highlights four EEG channels that are consistently identified

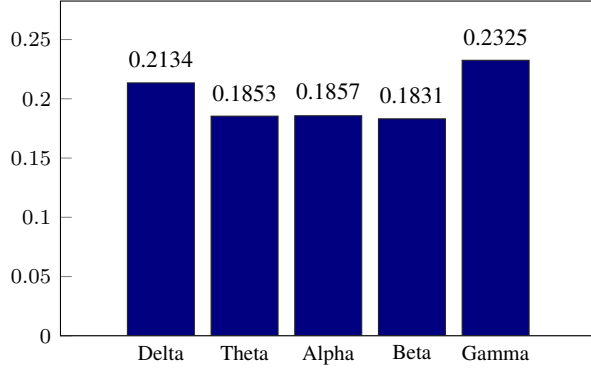


Fig. 4. Average importance of EEG frequency bands obtained by EGDA for cross-session emotion recognition

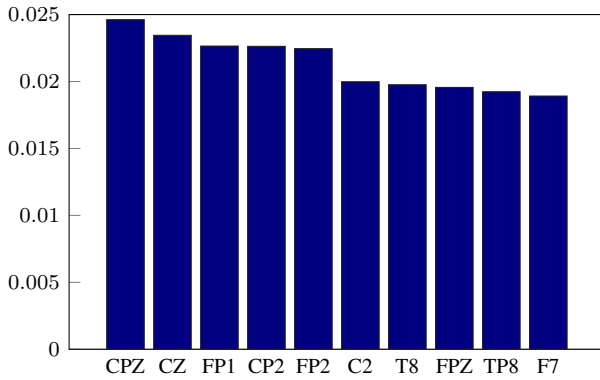


Fig. 5. Average EEG channel importance obtained by EGDA for cross-session emotion recognition.

as the most discriminative across all trials. These findings are consistent with previous studies, confirming the critical role of these brain regions in emotional processing [22].

V. CONCLUSION

In this work, we proposed EGDA framework for robust cross-session emotion recognition. The proposed method integrates distribution alignment with graph regularization to simultaneously reduce marginal and conditional discrepancies across sessions. By minimizing within-class scatter matrices in

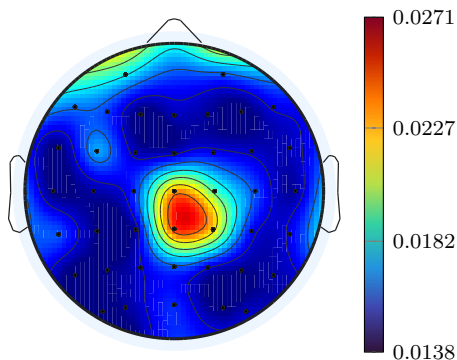


Fig. 6. The topographical show of the average Importance channel of EGDA for cross-session EEG emotion recognition.

- Session 1 → Session 2
- Session 1 → Session 3
- Session 2 → Session 3

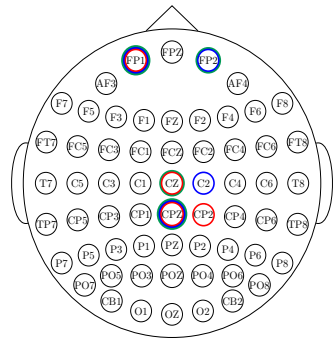


Fig. 7. The four most important EEG channels selected for each cross-session experiment.

the source domain, EGDA encourages compact and discriminative feature representations, thereby facilitating more effective domain adaptation. Experimental results on the SEED-IV dataset demonstrate that EGDA achieves superior recognition accuracy compared with several state-of-the-art baseline methods. Furthermore, our analysis highlights the Gamma frequency band as the most discriminative and identifies the prefrontal, central-parietal, and temporal brain regions as critical for emotional processing.

REFERENCES

- [1] R. W. Picard, *Affective computing*, MIT press, 2000.
- [2] H. A. Hamzah and K. K. Abdalla, “Eeg-based emotion recognition systems; comprehensive study,” *Helijon*, vol. 10, no. 10, 2024.
- [3] Z. He, Z. Li, F. Yang, L. Wang, J. Li, C. Zhou, and J. Pan, “Advances in multimodal emotion recognition based on brain–computer interfaces,” *Brain sciences*, vol. 10, no. 10, p. 687, 2020.
- [4] Y. Ding, N. Robinson, S. Zhang, Q. Zeng, and C. Guan, “Tsception: Capturing temporal dynamics and spatial asymmetry from eeg for emotion recognition,” *IEEE Transactions on Affective Computing*, vol. 14, no. 3, pp. 2238–2250, 2022.
- [5] V. Jayaram, M. Alamgir, Y. Altun, B. Scholkopf, and M. Grosses-Wentrup, “Transfer learning in brain-computer interfaces,” *IEEE Computational Intelligence Magazine*, vol. 11, no. 1, pp. 20–31, 2016.
- [6] W.-L. Zheng, W. Liu, Y. Lu, B.-L. Lu, and A. Cichocki, “Emotionmeter: A multimodal framework for recognizing human emotions,” *IEEE transactions on cybernetics*, vol. 49, no. 3, pp. 1110–1122, 2018.
- [7] W.-L. Zheng and B.-L. Lu, “Personalizing eeg-based affective models with transfer learning,” in *Proceedings of the twenty-fifth international joint conference on artificial intelligence*, pp. 2732–2738, 2016.
- [8] C. Liu, X. Zhou, Y. Wu, Y. Ding, L. Zhai, K. Wang, Z. Jia, and Y. Liu, “A comprehensive survey on eeg-based emotion recognition: A graph-based perspective,” *arXiv preprint arXiv:2408.06027*, 2024.
- [9] Y. Peng, F. Qin, W. Kong, Y. Ge, F. Nie, and A. Cichocki, “Gfil: A unified framework for the importance analysis of features, frequency bands, and channels in eeg-based emotion recognition,” *IEEE Transactions on Cognitive and Developmental Systems*, vol. 14, no. 3, pp. 935–947, 2021.
- [10] X. Li, Y. Zhang, Y. Peng, and W. Kong, “Enhanced performance of eeg-based brain–computer interfaces by joint sample and feature importance assessment,” *Health Information Science and Systems*, vol. 12, no. 1, p. 9, 2024.
- [11] Y. Peng, F. Jin, W. Kong, F. Nie, B.-L. Lu, and A. Cichocki, “Ogssl: A semi-supervised classification model coupled with optimal graph learning for eeg emotion recognition,” *IEEE Transactions on Neural Systems and Rehabilitation Engineering*, vol. 30, pp. 1288–1297, 2022.
- [12] T. Sha, Y. Zhang, Y. Peng, and W. Kong, “Semi-supervised regression with adaptive graph learning for eeg-based emotion recognition,” *Math. Biosci. Eng.*, vol. 20, no. 6, pp. 11379–11402, 2023.

- [13] F. Jin, Y. Peng, F. Qin, J. Li, and W. Kong, "Graph adaptive semi-supervised discriminative subspace learning for eeg emotion recognition," *Journal of King Saud University-Computer and Information Sciences*, vol. 35, no. 8, p. 101648, 2023.
- [14] F. Shen, Y. Peng, G. Dai, B. Lu, and W. Kong, "Coupled projection transfer metric learning for cross-session emotion recognition from eeg," *Systems*, vol. 10, no. 2, p. 47, 2022.
- [15] Y. Peng, W. Wang, W. Kong, F. Nie, B.-L. Lu, and A. Cichocki, "Joint feature adaptation and graph adaptive label propagation for cross-subject emotion recognition from eeg signals," *IEEE Transactions on Affective Computing*, vol. 13, no. 4, pp. 1941–1958, 2022.
- [16] S. J. Pan, I. W. Tsang, J. T. Kwok, and Q. Yang, "Domain adaptation via transfer component analysis," *IEEE transactions on neural networks*, vol. 22, no. 2, pp. 199–210, 2010.
- [17] M. Long, J. Wang, G. Ding, J. Sun, and P. S. Yu, "Transfer feature learning with joint distribution adaptation," in *Proceedings of the IEEE international conference on computer vision*, pp. 2200–2207, 2013.
- [18] J. Tahmoresnezhad and S. Hashemi, "Visual domain adaptation via transfer feature learning," *Knowledge and information systems*, vol. 50, no. 2, pp. 585–605, 2017.
- [19] F. Nie, X. Wang, and H. Huang, "Clustering and projected clustering with adaptive neighbors," in *Proceedings of the 20th ACM SIGKDD international conference on Knowledge discovery and data mining*, pp. 977–986, 2014.
- [20] Y. Peng, X. Zhu, F. Nie, W. Kong, and Y. Ge, "Fuzzy graph clustering," *Information Sciences*, vol. 571, pp. 38–49, 2021.
- [21] B. Ghojogh, F. Karay, and M. Crowley, "Eigenvalue and generalized eigenvalue problems: tutorial (2023)," *arXiv preprint arXiv:1903.11240*, 1903.
- [22] J. Zhang and P. Chen, "Selection of optimal eeg electrodes for human emotion recognition. ifac-papers on line, 53 (2), 10229–10235," 2020.